The Institution of Engineering and Technology

RPG 2022
Renewable Power Generation

22-23 September 2022

Meeting net zero carbon

Savoy Place, London

Call for papers deadline:
10 December 2021

#RPGLondon

Received: 11 February 2021 | Revised: 16 May 2021 | Accepted: 30 May 2021

IET Renewable Power Generation

DOI: 10.1049/rpg2.12232

The Institution of Engineering and Technology WILEY

ORIGINAL RESEARCH PAPER

A new relaying scheme for protection of transmission lines connected to DFIG-based wind farms

Javad Zare | **Sahar Pirooz Azad**

Department of Electrical and Computer Engineering, University of Waterloo, Waterloo, Ontario, Canada

Correspondence
Sahar Pirooz Azad, Department of Electrical and Computer Engineering, University of Waterloo, 200 University Avenue West, Waterloo, Ontario, Canada.
Email: sahar.azad@uwaterloo.ca

Abstract

This paper presents a new protection scheme with low communication capacity requirement for protecting lines connected to a doubly-fed induction generator (DFIG)-based wind farm (WF). The proposed relaying scheme addresses the line protection challenges which stem from the non-synchronous frequency component of the current fed from a DFIG-based WF during a short-circuit fault. The fault current frequency of a DFIG-based WF deviates from the synchronous frequency during a fault, which affects the operation of distance relays. In such a scenario, the distance relay located at the WF terminal may lose its coordination with downstream relays, resulting in unnecessary tripping. The proposed scheme relies on the impedance trajectory captured by the local relay, local fault current characteristics, and the frequency tracking of the fault current measured at the distance relays located at the two ends of the transmission line connected to a DFIG-based WF. The reliable performance of the proposed scheme is verified on a 4-bus test system under balanced and unbalanced faults during super- and sub-synchronous operating modes of the DFIG as well as its robustness against power system disturbances.

1 | INTRODUCTION

In modern power systems, wind energy sources are increasingly being integrated into transmission and distribution systems worldwide [1]. Three types of wind power generators are installed in power systems including the doubly-fed induction generator (DFIG), the squirrel cage induction generator (SCIG), and the full-scale converter-interfaced synchronous generator (CISG) [2, 3]. DFIG-based wind farms (WFs) have been widely utilised in power systems and comprise a considerable share of the installed capacity of the electricity generation worldwide, due to their many advantages such as variable speed operation, generator-side active power controllability, and grid-side reactive power controllability [3, 4].

With the large integration of WFs in the power grid, the fault ride-through (FRT) requirement has become an essential part of modern grid codes to increase grid reliability and stability [5]. WFs with FRT capability are required to remain connected to the power grid during fault conditions for a specific period. This will result in WFs contributing to the fault current and changing the system fault current characteristics [6]. Such changes in the fault current characteristics significantly affect the operation of protection relays used for the protection of transmission lines connected to DFIG-based WFs during short-circuit faults [6].

The short-circuit behaviour of DFIG-based WFs and their impact on protection systems, due to changes in the slip in the range of ±30% [2], can be evaluated during the large slip and near-zero slip operating modes. During the large slip operation of a DFIG, the performance of a distance relay located at the terminal of the DFIG-based WF will be unreliable and insecure during balanced faults and severe unbalanced faults close to the WF [2, 7]. For a large slip value, when a balanced fault occurs on a transmission line connected to the DFIG-based WF, the frequency of the fault current injected by the DFIG-based WF deviates from the synchronous frequency [2]. On the other hand, the frequency of the voltage at the relay location follows the grid synchronous frequency [7]. As a distance relay operates based on the ratio of fundamental frequency components of voltage and current measurements at the relay location [9], the difference in the frequency of the voltage and current during a fault leads to malfunctioning of the distance relay [7]. The protection relay may face the same problem as that of a balanced fault in case of a severe unbalanced fault close to a DFIG-based WF [10]. During the near-zero slip operation of a DFIG,

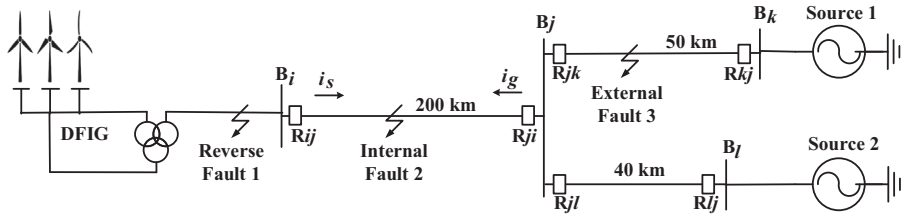

FIGURE 1 Single-line diagram of the test system

a conventional distance relay located at the DFIG terminal fails to operate correctly and loses coordination with downstream relays for a balanced fault in its backup zone due to the negligible magnitude of the fundamental component of the fault current after several hundred milliseconds [7].

The negative impacts of DFIG-based WFs on protection systems have been studied in [7, 11–21]. [7] proposes a pilot protective scheme based on the peak-to-peak value of the fault current injected by DFIG-based WFs. In the proposed method, fault current direction at the WF substation is detected using the shape of the fault current, while a conventional distance relay at the remote end of the line detects the fault direction by impedance measurement. [12–14] present a technique based on the modification of the trip boundary of a distance relay located at the terminal of a DFIG-based WF to address the distance relay failure. These adaptive setting schemes use the ratio of local voltage and current at the distance relay location. [11] proposes a pilot protection scheme based on exchanging the active power calculated at both ends of the transmission line to detect the location of the fault. [15] presents a new communication-based dual time-current-voltage scheme for directional overcurrent relays to determine the optimal relay tripping settings. [16] proposes an integrated DFIG protection scheme based on a modified superconducting magnetic energy storage-fault current limiter to control the rotor side converter. [17] proposes a protection scheme for DFIGs based on a resistive type superconducting fault current limiter connected in series with the DFIG rotor winding to limit the peak values of the rotor fault current and DC link voltage. In [18], a high-frequency fault component-based distance protection is presented to detect short-circuit faults in electrical systems with large renewable power plants. This method compares the magnitude of high-frequency operating voltage and high-frequency voltage to distinguish between internal and external faults. In [19], time-domain-based distance protection is presented using the R-L differential equation algorithm for transmission lines connected to DFIG-based WFs. This algorithm uses the memory voltage drop and actual voltage drop on the equivalent system impedance to detect the fault direction. [20] proposes a time-domain-based fault location algorithm using voltage and current signals measured at two ends of transmission lines connected to WFs. Voltage and current signals are sent to the other ends of the line using communication links. This method requires a half-cycle post-fault data window for fault location calculations. [21] presents a new time-domain protection algorithm for fault detection and location using fast discrete S-transform (FDST) for transmission lines connected to WFs.

The main drawbacks of the existing schemes for the protection of lines connected to DFIG-based WFs include (i) high communication bandwidth requirement for exchanging information between the relays at the two ends of the line connected to the DFIG-based WF [11, 15], (ii) inability to operate reliably in case of severe unbalanced faults close to the DFIG-based WF [7], (iii) requirement on the continuous availability of information about the DFIG-based WF such as the wind speed and the number of units in service to provide an adaptive relaying setting [12–14], (iv) high sampling frequency requirement [20, 21], and (v) failure to provide proper backup protection for the downstream relays in case of a balanced fault in zone 2 of a distance relay [12–14, 16–21].

In this paper, a new protection scheme, called modified distance element, with low communication capacity requirement is presented for protecting lines connected to a DFIG-based WF. The developed scheme relies on the local current and voltage measurements to detect and identify balanced and unbalanced faults when the DFIG operates at a near-zero slip value. In such a scenario, the impedance trajectory and fault current characteristic obtained from local measurements are used to differentiate between reverse, internal, and external faults as well as to provide backup protection for downstream relays. The modified distance element relies on tracking the frequency of the fault current at the two ends of the line to differentiate between internal and external faults when the DFIG operates at large slip values. By implementing the modified distance element in a 4-bus test system, it is verified that the new relaying scheme provides reliable protection over the entire length of the transmission line connected to the DFIG-based WF.

This paper is organised as follows, a brief description of the 4-bus test system is presented in Section 2. The protection challenges associated with transmission lines connected to DFIG-based WFs are discussed in Section 3. The modified distance element is described in Section 4. Study results and discussions are presented in Section 5. Conclusions are provided in Section 6.

2 | TEST SYSTEM

Figure 1 illustrates the single-line diagram of the 4-bus test system used in the studies of this paper. In this system, a DFIG-based WF is connected to bus i, and two identical sources with the same characteristics are connected to buses k and l. The parameters of the system are provided in Table 1. Further

TABLE 1 Parameters of the test system

Component	Parameter	Value
	Apparent power	5 MVA
	Nominal voltage	690 V
	Stator resistance	0.0054 p.u.
	Rotor resistance	0.00607 p.u.
DFIG-based WF	Magnetising inductance	4.5 p.u.
	Stator inductance	0.1 p.u.
	Rotor inductance	0.11 p.u.
	DC link rated voltage	1200 V
	DC link capacitor size	2 mF
	Nominal voltage	132 kV
Source	Positive-sequence impedance	$1\angle 80°$ p.u.
	Negative-sequence impedance	$1\angle 80°$ p.u.
	Zero-sequence impedance	$1.5\angle 80°$ p.u.
	Apparent power	5.5 MVA
DFIG transformer	Nominal voltage	690 V/900 V/33 kV
		YgYgYg
	Apparent power	50 MVA
Main transformer	Nominal voltage	33 kV/132 kV
		ΔYg
	Positive-sequence impedance	$0.1a44\angle 86°\ \Omega$/km
	Negative-sequence impedance	$0.144\angle 86°\ \Omega$/km
Transmission line	Zero-sequence impedance	$0.437\angle 86°\ \Omega$/km

information regarding the control system of the DFIG-based WF can be found in [27].

3 | PROTECTION CHALLENGES

In this section, the performance of a conventional distance relay located at the terminal of a DFIG-based WF during balanced and unbalanced faults is illustrated and the challenges associated with the protection of lines connected to DFIG-based WFs are described.

3.1 | Balanced faults

The balanced fault current of a DFIG-based WF is [2]

$$i_s(t) = \frac{V_{max}}{(1-s)\sqrt{X'^2 + R_{cb}^2}} \left[e^{-\frac{t}{T'_{cb}}} \times \cos\left((1-s)\omega_s t + \theta - \frac{\pi}{2}\right) - e^{-\frac{t}{T_s}} \cos\left(\theta - \frac{\pi}{2}\right)\right], \quad (1)$$

where T'_{cb} and T_s are the short-circuit transient and the stator time constants, respectively. V_{max}, X', R_{cb}, ω_s, s, and θ are the voltage amplitude, transient reactance, crowbar resistance, synchronous speed, machine slip, and fault inception angle, respectively. The fault current injected into the line from the AC grid is [2]

$$i_g(t) = \frac{V_{max}}{Z}[\sin(\omega_s t - \theta) - \sin(\theta) \times e^{-\frac{t}{T}}], \quad (2)$$

where T and Z are the time constant and equivalent impedance of the AC grid, respectively.

The negative impacts of a DFIG-based WF on distance relays during operation with large slip and near-zero slip values are as follows.

3.1.1 | Large slip operation

As the slip of a DFIG changes in the range of ±30%, the $(1-s)$ term in Equation (1) is considerable for large slip values. As a result, the fault current frequency injected by a DFIG-based WF changes in the range of 42–78 Hz for a 60 Hz system. On the other hand, during a balanced fault, the voltage frequency captured at the relay location follows the frequency of the AC grid and remains within a narrow margin of the synchronous frequency. Therefore, the frequency of voltage and current measured at the relay location will be different. This difference between the frequency of voltage and current negatively affects the performance of a distance relay.

The impedance measured by the phase-A-to-ground (AG) element of a conventional distance relay is calculated as [9]

$$Z_{AG} = \frac{V_A\angle\theta_v}{I_A\angle\theta_i + K_0 I_0}, \quad (3)$$

where $V_A\angle\theta_v$ and $I_A\angle\theta_i$ are the fundamental frequency phasors of the phase-A voltage and current, respectively. I_0 is the zero-sequence current, and K_0 is the zero-sequence compensation factor [9]. In a conventional distance relay used for protection of a line connected to a DFIG-based WF, due to the deviation of the fault current frequency from the synchronous frequency, the impedance value calculated by Equation (3) will not be an accurate estimation of the impedance between the fault and the relay location. This will result in the maloperation of the distance relay. The impedance trajectory measured by R_{ij} for a balanced fault at 40% of line *jk*, which is protected by zone 2 of R_{ij}, is presented in Figure 2.The impedance trajectory changes drastically and incorrectly enters zone 1 around 23 ms after onset of the fault, resulting in loss of coordination between R_{ij} and the downstream relays.

3.1.2 | Near-zero slip operation

During the DFIG operation at a near-zero slip, after a balanced fault in zone 2 of the WF-side distance relay, the fault current fed from the WF increases significantly for a short time period and the impedance calculated by the conventional distance relay

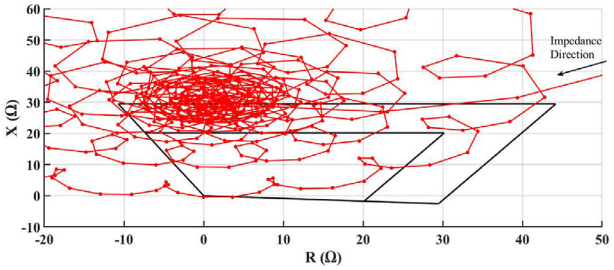

FIGURE 2 Impedance trajectory measured by the AG element of R_{ij} after a balanced fault at 40% of line jk ($s = -20\%$)

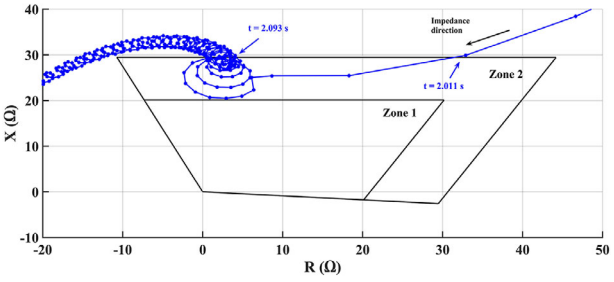

FIGURE 3 Impedance trajectory measured by the AG element of R_{ij} after a balanced fault at 50% of line jk ($s = 0$)

at the WF terminal correctly falls within zone 2 on the R–X plane. Then, the current decreases immediately due to a reduction in the generator's air-gap flux [26], which is caused by the significant voltage drop at the WF terminal [26]. A few hundred milliseconds after the balanced fault inception, the fault current reaches zero because of the complete demagnetisation of the core of the generator and the impedance trajectory finally leaves zone 2 of the distance relay [26]. As a result, the conventional distance relay cannot provide reliable protection in case of a balanced fault in its zone 2 as it must operate after a set time delay [9]. Figure 3 shows the impedance trajectory measured by R_{ij} for a balanced fault at 50% of line jk, which is protected by zone 2 of R_{ij} when the generator operates at $s = 0$. The impedance trajectory enters zone 2 and remains within zone 2 for around 82 ms and then leaves the protection zones; therefore, R_{ij} cannot provide reliable backup protection for the adjacent line.

3.2 | Unbalanced faults

A distance relay at the terminal of a DFIG-based WF may face the same problem as that of a balanced fault when a severe unbalanced fault occurs close to the DFIG. The approximate current injected by a DFIG-based WF for an unbalanced fault is calculated as follows [23]

$$i_{\mathrm{s}}(t) = i_{\mathrm{sf}}(t) + i_{\mathrm{sn}}(t)\,, \tag{4}$$

$$i_{\mathrm{sf}}(t) = \left(\frac{V_1}{jX'} - k_{\mathrm{r}} c \psi_{\mathrm{rf},1} L'_{\mathrm{s}}\right) e^{j\omega_{\mathrm{s}} t} + \frac{V_2}{Z_2} e^{-j\omega_{\mathrm{s}} t}\,, \tag{5}$$

$$i_{\mathrm{sn}}(t) = \frac{V_{\mathrm{pre}} - (V_1 - V_2)}{jX'} e^{-\frac{t}{T_{\mathrm{s}}}} - \frac{k_{\mathrm{r}}}{L'_{\mathrm{s}}}\left(d e^{-\frac{t}{T_{\mathrm{s}}}} + c e^{-\frac{t}{T'_{\mathrm{cb}}}} e^{j\omega_{\mathrm{r}} t}\right)\left(\psi_{\mathrm{r,pre}} - \left(\psi_{\mathrm{rf},1} + L_{\mathrm{r}2}\frac{V_2}{Z_2}\right)\right), \tag{6}$$

where V_{pre} is the pre-fault voltage, V_1 and V_2 are the positive- and negative-sequence voltages, respectively, and ω_{r} is the rotor angular frequency. $\psi_{\mathrm{r,pre}}$ and $\psi_{\mathrm{rf},1}$ are the pre-fault rotor flux and the positive-sequence component of the post-fault forced rotor flux, respectively. L'_{s}, $L_{\mathrm{r}2}$, and Z_2 are the transient inductance, negative-sequence rotor inductance, and total negative-sequence impedance of the generator, respectively. T_{s} is the stator time constant. i_{sn} and i_{sf} are respectively the natural and forced currents. Based on the constant flux linkage theorem [29], the stator flux is constant immediately after the onset of a fault; therefore, the stator natural flux is defined to compensate the difference between the stator forced flux before and after the fault. The details of calculating the stator natural and forced currents are provided in [23].

According to Equations (4)–(6), the fault current of a DFIG-based WF consists of a decaying dc component, a decaying AC component at the rotor frequency, and an AC component at the synchronous frequency. In Equations (4)–(6), the fault current is calculated by assuming the activation of the crowbar circuit due to the large negative-sequence current passing through the back-to-back converter for an unbalanced fault. When a severe unbalanced fault occurs close to the terminal of a DFIG-based WF, the terminal voltage drops significantly, resulting in small values for V_1 and V_2. These small voltages lead to a decrease in the magnitude of the AC component at the synchronous frequency and an increase in the magnitude of the decaying dc component and the decaying AC component at the rotor frequency according to Equation (6). Therefore, an unbalanced fault close to the relay results in a fault current with a considerable AC component with the rotor frequency. However, by moving the fault location away from the DFIG-based WF, the voltage sag will reduce; therefore, the fault current will be comprised of a larger AC component at the synchronous frequency.

To illustrate the impact of unbalanced faults on the protection of distance relays, the impedance trajectories measured by R_{ij} for a phase-A-to-phase-B-to-ground (ABG) fault at two different locations are shown in Figure 4. For the fault at the beginning of line ij, the impedance trajectory measured by R_{ij} correctly enters zone 1 and remains within zone 1 despite a small drifting due to the large decaying AC current component with the rotor frequency. This drifting does not affect the operation of R_{ij} as the fault has occurred in zone 1. For the fault at the beginning of line jk, the impedance trajectory correctly enters zone 2 and remains within zone 2 despite a small swing on the R–X plane due to the small decaying AC current component with the rotor frequency. Therefore, R_{ij} can provide proper backup protection for line jk during unbalanced faults.

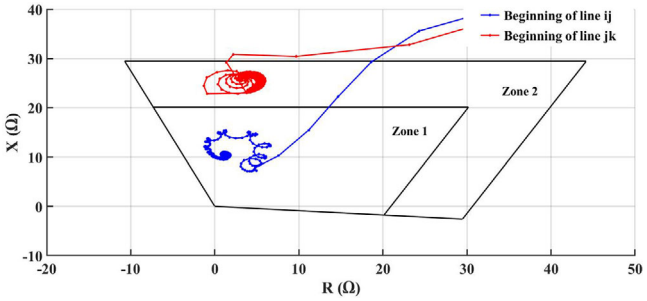

FIGURE 4 Impedance trajectory measured by the AG element of R_{ij} after an ABG fault at the beginning of line ij ($s = -30\%$)

4 | MODIFIED DISTANCE ELEMENT

In this section, a new protection scheme with low communication capacity requirement for protecting lines connected to DFIG-based WFs is presented to address the previously-discussed protection challenge arising from the non-synchronous frequency component of the fault current. The new relaying scheme, called modified distance element, relies on the impedance trajectory and the fault current characteristic obtained from local current and voltage measurements as well as the communication of a binary signal between the two ends of the transmission line. The binary signal is determined based on the fault current captured by the relay.

Figure 5 depicts the fault detection and identification process of the proposed relaying scheme implemented in R_{ij}. The modified distance element has two main components: (i) fault detection and (ii) fault type identification. In this scheme, local current and voltage measurements at the relay location are used to detect faults and distinguish them from disturbances such as power swings and load encroachments. After a fault is detected, a binary signal SR_{ij} is calculated, which depends on the frequency of the local current. This signal is used to distinguish between forward and reverse faults as well as to determine whether the DFIG operates in the near-zero or large slip range. When the DFIG operates at a large slip value, the protection scheme will rely on receiving the binary signal SR_{ji} from the remote end of the line to distinguish between forward internal and external faults. Reverse fault identification relies on the impedance trajectory. For the near-zero slip operation of the DFIG, first, balanced faults are identified from unbalanced faults. Then, a conventional distance element is used to identify the unbalanced faults and the zone where they have occurred. Forward balanced fault identification during the near-zero slip operation of the DFIG relies on the impedance trajectory and the local fault current waveform damping characteristics.

4.1 | Fault detection

The fault detection component distinguishes the fault condition from power system disturbances such as power swings and load encroachments. In this protection scheme, the fault detection scheme presented in [24], which is based on the asymmetry of the instantaneous fault current waveform after the onset of the fault, is used. This phenomenon is not observed during power swings, load encroachments, and normal operation of the power system. In this scheme, the one-cycle moving sum of the current samples is calculated. Because of the symmetric nature of the current waveform during normal operation of the power system, the moving sum of the samples becomes around zero. On the other hand, the moving sum of the samples deviates from zero in case of faults due to the large dc component of the fault current waveform [24].

4.2 | Fault type identification

The slip of a DFIG can change in the range of ±30%. In the proposed scheme, a suitable slip threshold s_{th} is defined to determine whether the fault current frequency f is within a predefined frequency bound.

$$-s_{th} \le s \le s_{th} , \tag{7}$$

$$f_{lb} \le f \le f_{ub} , \tag{8}$$

$$f_{lb} = (1 - s_{th}) f_s , \tag{9}$$

$$f_{ub} = (1 + s_{th}) f_s , \tag{10}$$

where f_{lb} and f_{ub} are the lower and upper bounds of the frequency, respectively. Near-zero slip operation of a DFIG is associated with the slip in the range of Equation (7), while any slip larger than s_{th} or less than $-s_{th}$ corresponds to the large slip operation of a DFIG.

The difference between the frequency of the fault current injected by a DFIG-based WF and an AC grid to the fault location is used to distinguish between internal and external faults. Two binary variables, SR_{ij} and SR_{ji}, are respectively defined based on the frequency of the fault current measured at R_{ij} and R_{ji}. When the fault current frequency measured at R_{ij} is within the range defined in Equation (8), SR_{ij} is set to zero, while it will become one if the fault current frequency is out of the range defined in Equation (8). There is a similar expression for SR_{ji} based on the fault current frequency measured at the remote relay. SR_{ij} (SR_{ji}) signal is communicated to the other end of the line to identify the fault location. After a fault, as shown in Figure 6, three scenarios will occur.

4.2.1 | $SR_{ij} = SR_{ji} = 0$

This scenario will happen if (i) a reverse fault occurs behind R_{ij} regardless of the DFIG's slip and the fault type, or (ii) DFIG operates at a near-zero slip within the range defined in Equation (7), regardless of the fault location.

In this fault scenario, the fault type (reverse, internal, or external) is identified based on the impedance measured at the relay

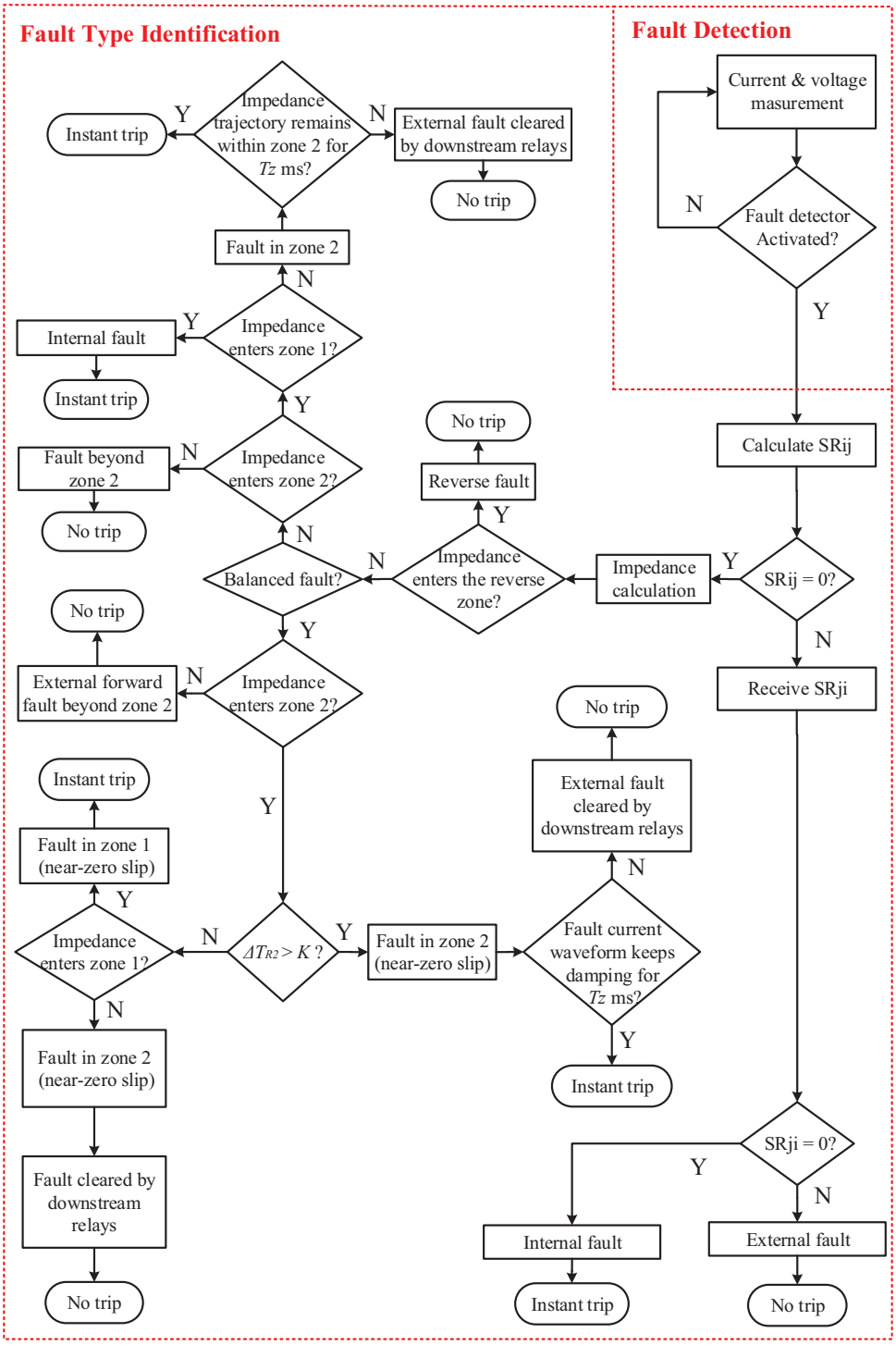

FIGURE 5 Modified distance element for the operation of R_{ij}

location together with the fault current waveforms injected by the WF. For forward fault identification, first, a fault type classifier is used to distinguish between balanced and unbalanced faults using an index called $FDC = \frac{NS_c}{PS_c}$, which is the ratio of the negative- (NS_c) and positive-sequence (PS_c) components of the fault current. FDC value for balanced faults is close to zero while it deviates from zero in case of unbalanced faults.

During unbalanced forward faults, the impedance trajectory does not leave zone 2 as the fault current waveform does not immediately decay to zero. The reason is that the air-gap flux in case of an unbalanced fault does not decrease as much as a balanced fault due to the higher voltage values in the healthy phases [28]. Conventional distance relaying algorithms such as [12] can be used in R_{ij} to provide reliable protection against unbalanced faults.

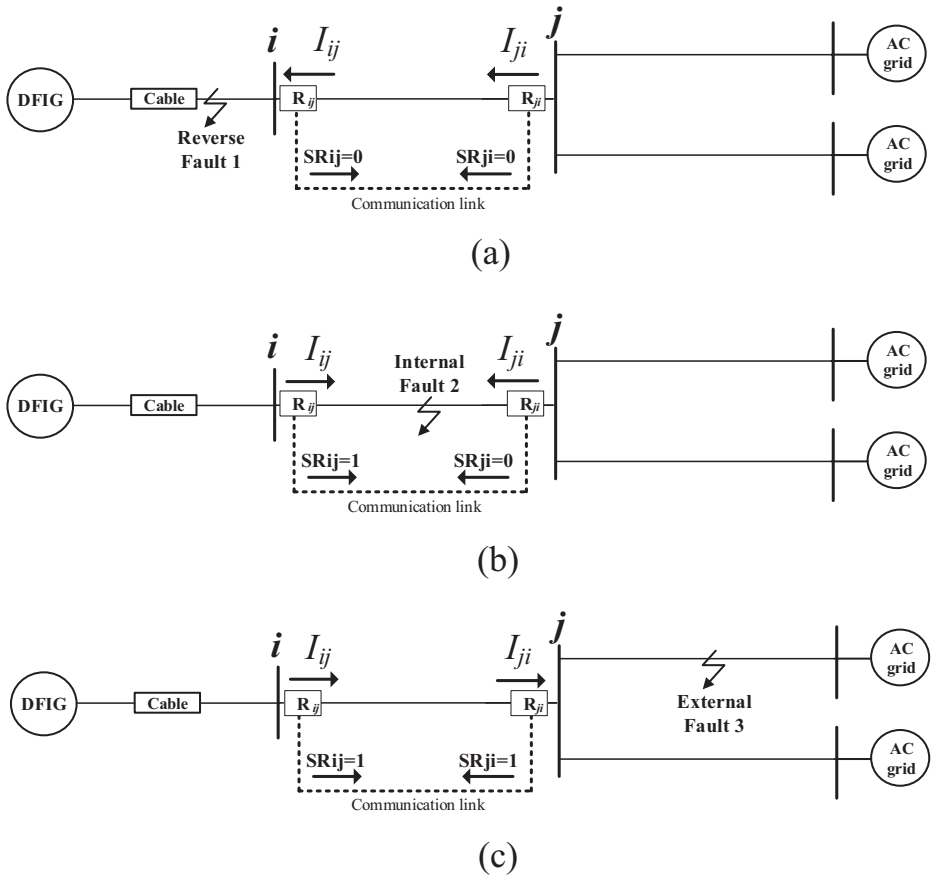

FIGURE 6 SR_{ij} and SR_{ji} after the occurrence of a balanced (a) reverse fault, (b) internal fault, and (c) external fault

During balanced forward faults in zone 2, after the fault inception, the impedance trajectory remains in zone 2 for a time period ΔT_{R2} (about a few cycles) without entering zone 1 due to the substantially large magnitude of the fault current. Comparison of ΔT_{R2} against a threshold K serves as the main criterion to distinguish between balanced faults in zone 1 and zone 2: If (i) $\Delta T_{R2} \leq K$ and the impedance trajectory enters zone 1, the fault is identified to be in zone 1, (ii) $\Delta T_{R2} \leq K$ and the impedance trajectory leaves zones 1 and 2, the fault is cleared by a downstream relay (e.g. R_{jk} or R_{jl} in Figure 1), and (iii) $\Delta T_{R2} \geq K$, the fault is identified to be in zone 2. Although in the third scenario, the impedance trajectory will remain within zone 2 for more than K ms, it will leave zone 2 before the time delay settings of this zone (T_{z2} ms) and therefore, the fault will not be detected by a conventional distance relay. To solve this problem, the relay will use the fault current waveform damping characteristic. If the current waveform continues to damp out for T_{z2} ms after the onset of the fault, the relay will operate after T_{z2} ms. However, for a fault already cleared by a downstream relay, the fault current does not damp out anymore.

K is selected as the shortest time period ΔT_{R2} for which the impedance trajectory remains in zone 2 for all uncleared balanced faults. This time period is associated with a balanced fault at the end of zone 2, which is not cleared by the downstream relays (R_{jk} or R_{jl}).

4.2.2 | $SR_{ij} = 1$ and $SR_{ji} = 0$

This scenario happens when the generator slip is out of the range defined in Equation (7) and a balanced internal fault occurs on the transmission line or a severe unbalanced fault occurs close to the DFIG terminal. In this fault scenario, the relays located at the two ends of the line must operate instantaneously.

4.2.3 | $SR_{ij} = SR_{ji} = 1$

In this scenario, the fault currents measured at the two ends of the line are injected by the DFIG-based WF and the wind turbine is operating with a slip out of the range defined in Equation (7); therefore, the fault is identified as an external fault.

5 | SIMULATION RESULTS

To investigate the performance of the modified distance element, the protection scheme is implemented in the test system shown in Figure 1. The test system is simulated in PSCAD and the currents and voltages at the distance relay location are sampled at 1000 Hz. Then, the current samples are imported to

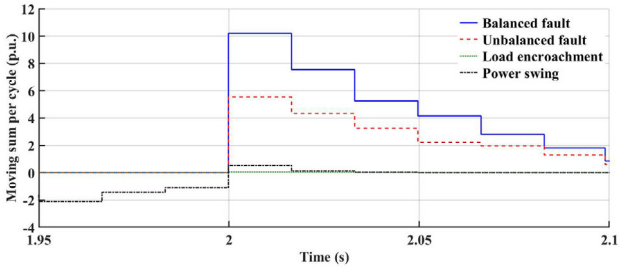

FIGURE 7 The moving sum over one cycle of the phase-A current

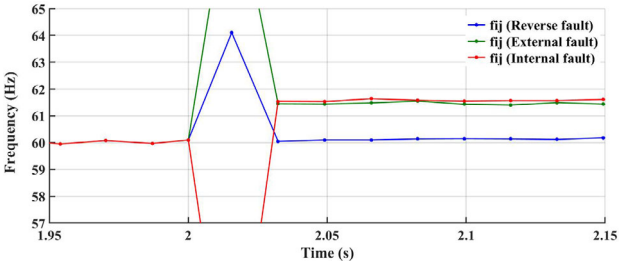

FIGURE 8 Frequency of I_{ij} for three fault scenarios ($s = -3\%$)

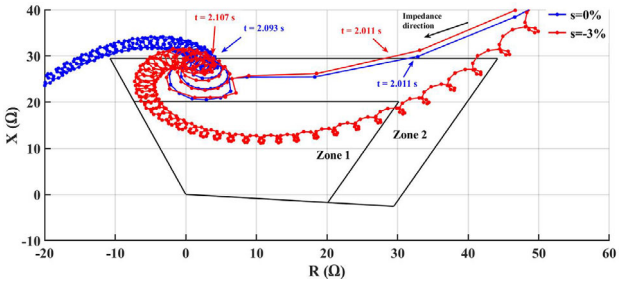

FIGURE 9 Impedance trajectories calculated by R_{ij} for a balanced external fault at 50% of line *jk*

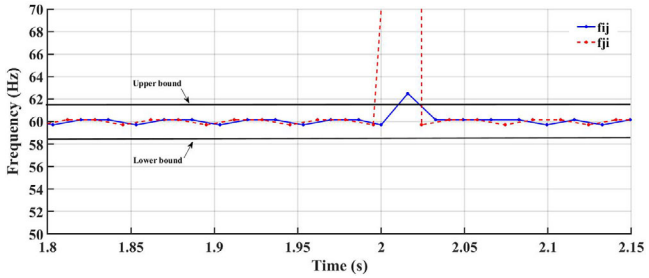

FIGURE 10 Frequency of I_{ij} and I_{ji} for a balanced reverse fault at the WF terminal ($s = -20\%$)

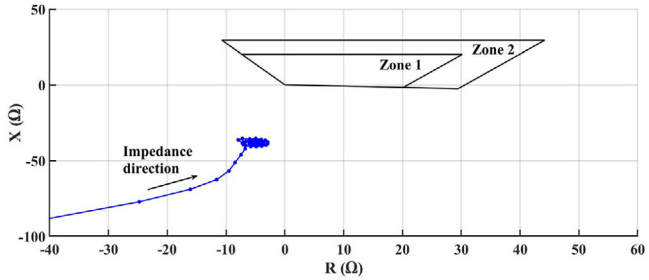

FIGURE 11 Impedance trajectory calculated by R_{ij} for a balanced reverse fault at the WF terminal ($s = -20\%$)

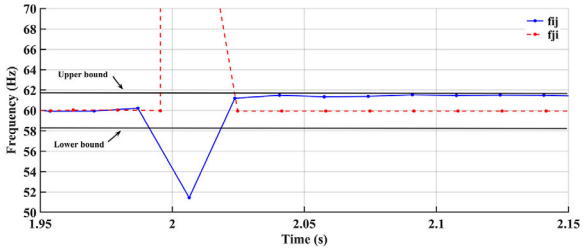

FIGURE 12 Frequency of I_{ij} and I_{ji} for a fault at the end of the line *ij* ($s = -3\%$)

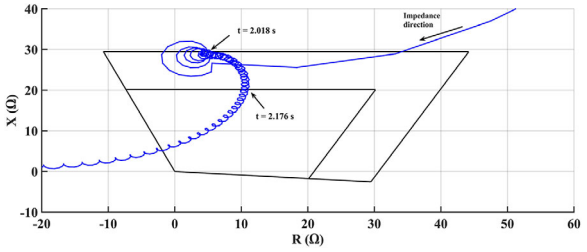

FIGURE 13 Impedance trajectory calculated by R_{ij} for a balanced fault at the end of line *ij* ($s = -3\%$)

MATLAB and one-cycle fast Fourier transform (FFT) is used to calculate the frequency of the current.

5.1 | Fault detection

The test system is studied under four scenarios including two short-circuit faults, a power swing, and a load encroachment. Two fault scenarios, a balanced fault and an AG fault at the end

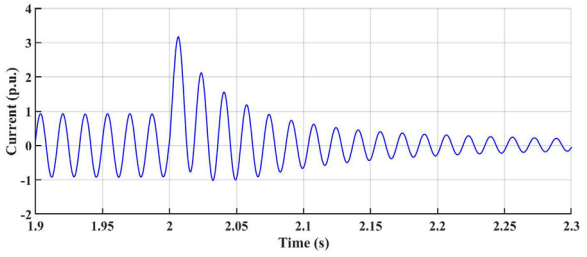

FIGURE 14 Fault current measured at R_{ij} for a balanced fault at the end of line *ij* ($s = -3\%$)

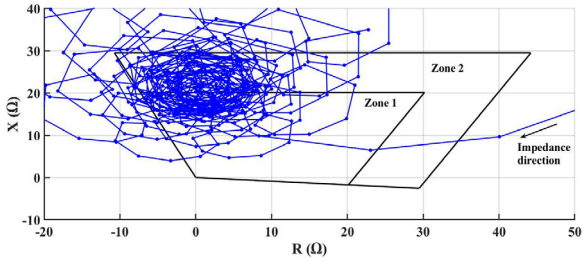

FIGURE 15 Impedance trajectory calculated by R_{ij} for a balanced internal fault at the end of line *ij* ($s = -30\%$)

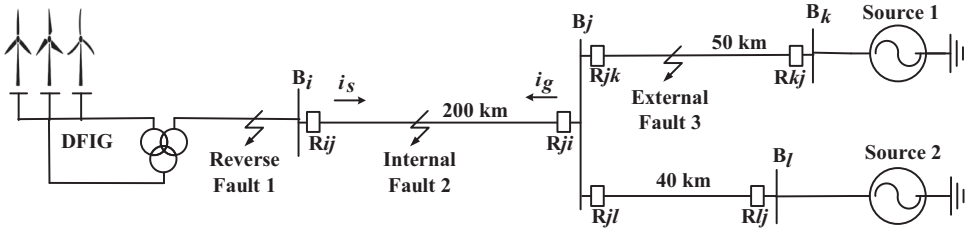

FIGURE 16 Frequency of I_{ij} and I_{ji} for a balanced internal fault at the end of line ij ($s = -30\%$)

FIGURE 17 Impedance trajectory calculated by R_{ij} for a balanced external fault at 50% of line jk ($s = -30\%$)

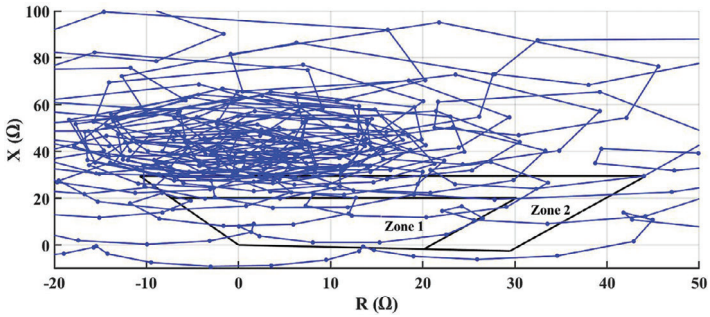

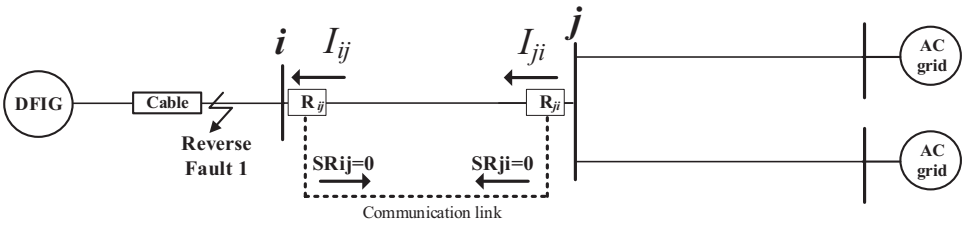

(a)

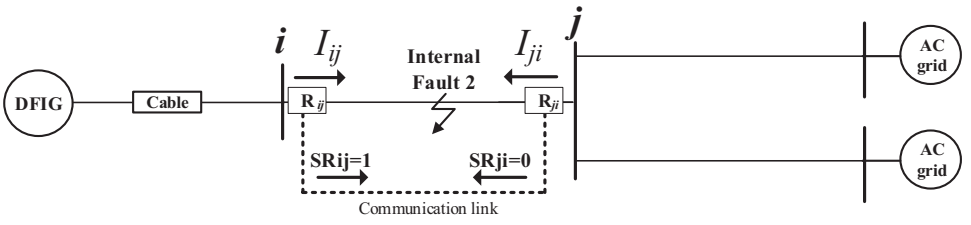

(b)

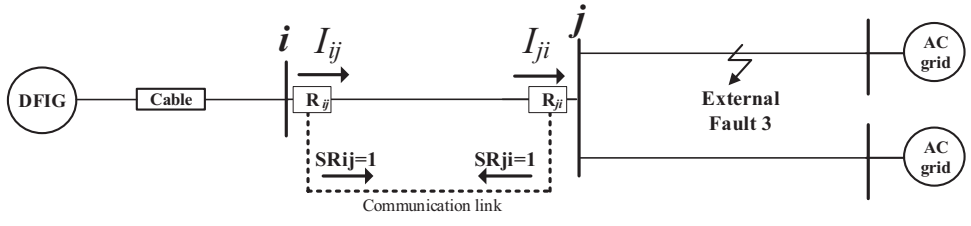

(c)

FIGURE 18 Frequency of I_{ij} and I_{ji} for a balanced external fault at 50% of line jk ($s = -30\%$)

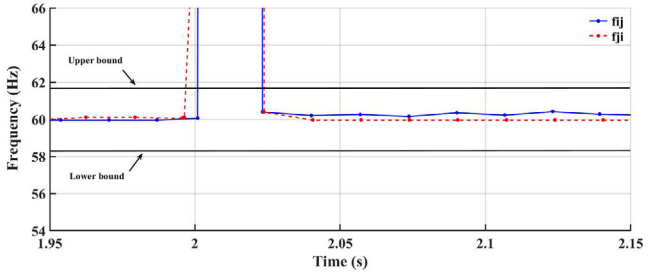

FIGURE 19 Frequency of I_{ij} and I_{ji} for an ABG fault at the beginning of zone 2 ($s = -30\%$)

of line ij at $t = 2$ s with $R_f = 1\ \Omega$, are considered. To create a power swing condition in the system, a transmission line parallel with line ij and with similar characteristics is added to the system. Then, a balanced fault at the middle of the new line is initiated at $t = 1.9$ s and is removed at $t = 2$ s by opening the circuit breakers located at the two sides of the new line. For simulating the load encroachment condition, a new load (100 MW and 25 MVAR) is connected to bus j at $t = 2$ s.

According to Figure 7, the moving sum has a significant value only for balanced and unbalanced faults. The non-zero value of the moving sum for the power swing scenario before $t = 2$ s is due to fault on the parallel line for creating the power swing after $t = 2$ s.

5.2 | Relay setting

The modified distance element has two settings s_{th} and K that should be selected according to the system parameters.

5.2.1 | Selection of s_{th}

When the DFIG operates at a near-zero slip value, the fault current of the DFIG is dominated by the AC component at the synchronous frequency [23, 25]. The upper bound of the slip range corresponds to the maximum slip value associated with the reliable operation of the modified distance element for DFIG operation at near-zero slip values. In other words, when the DFIG operates at any slip value lower than the upper bound, the impedance trajectory associated with a balanced fault in zone 2 of R_{ij} will remain in zone 2 for sufficient time such that the modified distance element can reliably detect the fault.

On the other hand, the upper bound of the slip range should be selected to be large enough so that the modified distance element can reliably identify the type of the fault, i.e. reverse, internal, or external. In other words, when the DFIG operates at any slip value higher than the upper bound, the current frequency difference between reverse and forward faults is sufficiently large.

Figure 8 illustrates the fault current frequency associated with three different faults when the DFIG operates at $s = -3\%$: (i) a balanced reverse fault behind the relay at the DFIG terminal, (ii) a balanced internal fault at the end of line ij, and (iii) a balanced external fault at 50% of line jk. The second and third faults result in the smallest magnitude of the current component with the non-synchronous frequency compared to other internal and external faults, respectively and consequently are the most difficult faults to be detected. According to Figure 8, the difference between the fault current frequency associated with these faults is about 1.3 Hz, which results in sufficient frequency deviation to distinguish reverse faults from forward faults. Therefore, for the test systems of this paper, $s_{th} = 3\%$ is selected ($f_{ub} = 61.8$ Hz and $f_{lb} = 58.2$ Hz).It should be noted that s_{th} depends on the electrical system under study.

5.2.2 | Selection of K

K is selected as the shortest time period for which the impedance trajectory remains in zone 2 for an uncleared balanced fault when the DFIG operates at near-zero slip values. For super- and sub-synchronous operating modes of the DFIG, the shortest time period is associated with a balanced fault at the end of zone 2 (50% of the largest adjacent line), which results in the smallest fault current. As explained in [22], a smaller fault current results in a larger error in the impedance measured by the distance relay and consequently, faster departure of the impedance trajectory from zone 2 in the R–X plane. The fault current is also inversely proportional to $(1 - s)$. Therefore, for the super-synchronous operation of the generator at $-s_{th} \le s < 0$, the fault current will have the smallest value for $s = -s_{th} = -3\%$. Also, for the sub-synchronous operation of the generator at $0 \le s < s_{th}$, the fault current will have the smallest magnitude at $s = 0$.

Figure 9 shows the impedance trajectories associated with faults at the end of zone 2 for $s = -3\%$ and $s = 0$. During the super-synchronous operation of the generator, the impedance trajectory enters zone 2 and remains within zone 2 for $\Delta T_{R2} = 96$ ms and then incorrectly enters zone 1. For the sub-synchronous operation of the generator, on the other hand, the impedance trajectory enters zone 2 and remains within zone 2 for $\Delta T_{R2} = 82$ ms and then leaves the relay zones. Therefore, $K = 80$ ms is selected for the test system of this paper.

5.3 | Fault type identification

To evaluate the performance of the fault type identification component, five fault conditions are studied:

5.3.1 | Balanced reverse fault

A balanced reverse fault on the terminal of the DFIG-based WF with $R_f = 1\ \Omega$ is studied when the generator is operating at $s = -20\%$. The fault current frequency observed by R_{ij} remains near 60 Hz, Figure 10, resulting in $SR_{ij} = 0$. According to Figure 10, the first frequency sample calculated right after the fault is not a good representation of the current frequency during the fault as it is based on the one-cycle of the current measurement,

where the first half-cycle corresponds to the pre-fault period and the second half-cycle is associated with the fault duration. Therefore, SR_{ij} (SR_{ji}) signal becomes one only if the measured frequency is out of the pre-defined range of Equation (8) for more than one sample. The impedance trajectory calculated by R_{ij} is shown in Figure 11. The impedance trajectory lies in the third quadrant of the R–X diagram, where it is covered by the reverse zone of R_{ij}; therefore, R_{ij} does not operate.

5.3.2 | Balanced internal fault when the generator operates at a near-zero slip value

A balanced fault at the end of line ij is studied when the generator is operating at $s = -3\%$ as this is associated with the maximum deviation of the fault current frequency from the synchronous frequency as well as the lowest current value among $|s| \leq s_{th}$ based on Equation (1). The frequency of I_{ij}, as shown in Figure 12, remains within the pre-defined frequency bounds; therefore, $SR_{ij} = 0$. The impedance trajectory calculated by R_{ij} correctly enters zone 2 and remains within zone 2 for $\Delta T_{R2} = 158$ ms before entering zone 1, Figure 13. Since $\Delta T_{R2} \geq K = 80$ ms, the fault current damping will be used to distinguish existing faults from those cleared by the downstream relays. Based on Figure 14, the fault current waveform captured by R_{ij} keeps damping for more than 300 ms (the time delay setting for zone 2), resulting in tripping R_{ij} after this time delay.

5.3.3 | Balanced internal fault when the generator operates at a high slip value

An internal fault at the end of line ij is studied when the generator operates at $s = -30\%$. This fault condition is the one which results in the maximum fault current frequency deviation as well as the lowest fault current value. Figure 15 illustrates the inability of the conventional distance relay to measure the correct impedance from the relay location to the fault location due to the non-synchronous frequency of the fault current injected by the DFIG-based WF. The frequency of the fault current measured at R_{ij} deviates significantly from the synchronous frequency and is out of the frequency bounds (58.2 Hz $\leq f_{ij} \leq$ 61.8 Hz) for more than one sample, while the fault current frequency at R_{ji} remains within the frequency bounds, Figure 16. Therefore, $SR_{ij} = 1$ and $SR_{ji} = 0$, which results in correct identification of the internal fault by R_{ij} and R_{ji}.

5.3.4 | Balanced external fault in zone 2 of R_{ij}

A balanced fault at 50% of line jk is studied when the generator operates at $s = -30\%$ in which the fault current measured by R_{ij} has the maximum frequency deviation and the lowest value for an external fault in zone 2 of R_{ij}. Although this is an external fault in zone 2 of R_{ij}, the impedance trajectory enters zone 1, Figure 17, and therefore, a conventional distance relay fails to correctly identify the fault and loses coordination with R_{jk}. Figure 18 shows the frequency of the fault currents deviates from the synchronous frequency and is out of the frequency bounds (58.2 Hz $\leq f_{ij} \leq$ 61.8 Hz). Therefore, $SR_{ij} = SR_{ji} = 1$, and the fault is correctly identified as an external fault with the modified distance element.

5.3.5 | Unbalanced fault

An ABG fault at the beginning of line jk is studied when the generator operates at $s = -30\%$. The frequency of I_{ij} remains within the pre-defined frequency bounds, Figure 19; therefore, $SR_{ij} = 0$. The impedance trajectory measured by R_{ij} enters zone 2 and remains within zone 2, Figure 4. Therefore, R_{ij} correctly operates as a backup after the time delay set for zone 2 operation.

6 | CONCLUSION

This paper presented a new protection scheme, called modified distance element, for protecting lines connected to DFIG-based WFs. The developed scheme relies on the impedance trajectory, fault current waveform damping characteristics, and the frequency tracking of the fault current injected by the DFIG. The performance of the modified distance element has been examined on a 4-bus test system. Based on a comprehensive suite of simulation studies, the main features of the modified distance element can be summarised as follows:

- Low communication bandwidth requirement;
- Provision of reliable protection over the entire length of transmission line connected to a DFIG-based WF;
- Robustness against different system disturbances such as power swings and load encroachments;
- Provision of backup protection for adjacent lines when the DFIG operates at near-zero slip; and
- Provision of reliable protection when the DFIG operates at super- and sub-synchronous speeds.

ORCID

Javad Zare https://orcid.org/0000-0003-3660-2276
Sahar Pirooz Azad https://orcid.org/0000-0002-6194-4182

REFERENCES

1. Ackermann, T.: Wind Power in Power Systems, 2nd ed, ch. 5. Wiley/Blackwell, Hoboken, NJ (2012)
2. Tleis, N.D.: Power Systems Modelling and Fault Analysis, ch. 5. Newnes, Oxford (2008)
3. Wu, B. et al.: Power Conversion and Control of Wind Energy Systems, vol. 76. Wiley, New York (2011)
4. Chen, H., Aliprantis, D.C.: Analysis of squirrel-cage induction generator with Vienna rectifier for wind energy conversion system. IEEE Trans. Energy Convers. 26(3), 967–975 (2011)
5. Tsili, M., Papathanassiou, S.: A review of grid code technical requirements for wind farms. IET Renewable Power Gen. 3(3), 308–332 (2009)
6. Muljadi, E., et al.: Effect of variable speed wind turbine generator on stability of a weak grid. IEEE Trans. Energy Convers. 22(1), 29–36 (2007)

7. Hooshyar, A., Azzouz, M.A., El-Saadany, E.F.: Distance protection of lines connected to induction generator-based wind farms during balanced faults. IEEE Trans. Sustain. Energy 5(4), 1193–1203 (2014)
8. Morren, J., de Haan, S.W.H.: Short-circuit current of wind turbines with doubly fed induction generator. IEEE Trans. Energy Convers. 22(1), 174–180 (2007)
9. Horowitz, S.H., Phadke, A.G.: Power System Relaying, vol. 22. Wiley, New York (2008)
10. Li, B. et al.: Fault studies and distance protection of transmission lines connected to DFIG-based wind farms. 8(4), 562 (2018)
11. Ghorbani, A., Mehrjerdi, H., Al-Emadi, N.A.: Distance-differential protection of transmission lines connected to wind farms. Int. J. Electr. Power Energy Syst. 89, 11–18 (2017)
12. Pradhan, A., Joos, G.: Adaptive distance relay setting for lines connecting wind farms. IEEE Trans. Energy Convers. 22(1), 206–213 (2007)
13. Dubey, R., Samantaray, S.R., Panigrahi, B.K.: Adaptive distance protection scheme for shunt-facts compensated line connecting wind farm. IET Gen. Trans. Dist. 10(1), 247–256 (2016)
14. Dubey, R., Samantaray, S.R., Panigrahi, B.K.: Simultaneous impact of unified power flow controller and off-shore wind penetration on distance relay characteristics. IET Gen. Trans. Dist. 8(11), 1869–1880 (2014)
15. Saleh, K.A., Moursi, M.S.E., Zeineldin, H.H.: A new protection scheme considering fault ride through requirements for transmission level interconnected wind parks. IEEE Trans. Ind. Informatics 11(6), 1324–1333 (2015)
16. Xiao, X., et al.: Integrated DFIG protection with a modified SMES-FCL under symmetrical and asymmetrical faults. IEEE Trans. Appl. Supercond. 28(4), 1–6 (2018)
17. Zou, Z., et al.: Integrated protection of DFIG-based wind turbine with a resistive-type SFCL under symmetrical and asymmetrical faults. IEEE Trans. Appl. Supercond. 26(7), 1–5 (2016)
18. Yang, Z., et al.: High-frequency fault component-based distance protection for large renewable power plants. IEEE Trans. on Power Electronics 35(10), 10352–10362 (2020)
19. Chen, Y. et al.: Distance protection for transmission lines of DFIG-based wind power integration system. Int. J. Electr. Power Energy Syst. 438–448 (2018)
20. Mahfouz Aly, M.M.A., El-Sayed, M.A.H.: Enhanced fault location algorithm for smart grid containing wind farm using wireless communication facilities. IET Gen. Trans. Dist. 10, 2231–2239 (2016)
21. Sahoo, B., Samantaray, S.R.: An enhanced fault detection and location estimation method for TCSC compensated line connecting wind farm. Int. J. Electr. Power Energy Syst. 432–441 (2018)
22. Zare, J., Azad, S.P.: A new distance protection scheme for SCIG-based wind farms. In: 2020 IEEE Power and Energy Society General Meeting, pp. 1–5. IEEE, Piscataway, NJ (2020).
23. Sulla, F., Svensson, J., Samuelsson, O.: Symmetrical and unsymmetrical short-circuit current of squirrel-cage and doubly-fed induction generators. Electr. Power Syst. Res. 81(7), 1610–1618 (2011)
24. Pradhan, A.K., Routray, A., Mohanty, S.R.: A moving sum approach for fault detection of power systems. Electr. Power Compon. Syst. 34(4), 385–399 (2006)
25. Tu, Q. et al.: Short-circuit sequence network model of DFIG with different slips. In: 2018 IEEE Power Energy Society General Meeting, pp. 1–5. IEEE, Piscataway, NJ (2018)
26. Hansen, A.D.: Generators and power electronics for wind turbines. Wind Power in Power Systems, pp. 53–78. Wiley, New York (2005)
27. https://hvdc.ca/knowledge-base/read,article/496/type-3-wind-turbine-generators-wtg-for-pscad-v4-6/v
28. Chen, X.S. et al.: Digital modeling of an induction generator. In: 1991 International Conference on Advances in Power System Control, Operation and Management, pp. 720–726. IEEE, Piscataway, NJ (1991)
29. Doherty, R.E., Nickle, C.A.: Three-phase short circuit synchronous machines–Part V. Trans. AIEE 49(2), 700–714 (1930)

How to cite this article: Zare, J., Pirooz Azad, S.: A new relaying scheme for protection of transmission lines connected to DFIG-based wind farms. IET Renew. Power Gener. 15, 2971–2982 (2021). https://doi.org/10.1049/rpg2.12232